Supplemental Material

Ranolazine for congenital and acquired late I_{Na} linked arrhythmias: *in silico* pharmacologic screening

Jonathan D. Moreno, MD, PhD, Pei-Chi Yang, PhD, John R. Bankston, PhD, Eleonora Grandi, PhD, Donald M. Bers PhD, Robert S. Kass, PhD, and Colleen E. Clancy, PhD

Materials and Methods Summary

A computational Markov model of the WT ranolazine, ΔKPQ drug-free, and ΔKPQ ranolazine, drug channel interaction was formulated via numerical optimization from experimentally derived rate constants as previously described [1]. Channel models recapitulated many features of Na^+ channel blockade including time and voltage dependent recovery, frequency and use-dependent block, as well as tonic block. The drug channel model was incorporated into a computational model of the human ventricular myocyte as described previously [1]. All source code used for simulations in this paper is available upon request. Full methods are below.

Full Materials and Methods

Simulations were encoded in C/C++ and run on a Sun Fire X4440 x64 Server and multiple Apple Intel based Mac Pros 3.0 GHz 8-Core using OpenMP with the Intel ICC compiler version 11.1. Numerical results were visualized using MATLAB R2012a by The Math Works, Inc. All parameter optimization source code used in this paper is available and can be obtained by emailing ceclancy@ucdavis.edu.

Inclusion of Bursting States in the Wild-Type Model

The wild-type drug-free model was used as previously described [1], but now includes a bursting regime. To model bursting states, a "burst" mode of gating from C3, C2, C1, and O, that includes 3 closed states and an open state is added to the model, and denoted with the prefix *B* (***B***C3, ***B***C2, ***B***C1, ***B***O). The rates governing the transition between background and burst modes (μ1 = entry into bursting mode, μ2 = egress from bursting mode) are time independent and represent the probability of transitioning between the two modes of gating. Initial estimates were taken from [2]. The bursting rate constants (μ1 and μ2) were optimized (all other rate constants held constant) to yield a sustained inward current of ~0.1% of the peak Na^+ current at tonic pacing (BCL = 3000) for WT, and a sustained inward current of 1% for the heart failure (HF) model. Further details about modeling sustained inward Na current can be found in Clancy et al. [2].

Online Table I

Transition rates Drug free WT Na^+ channel (ms^{-1})	
IC3 →IC2, C3→C2	α11= 8.5539/(7.4392e-2*exp(-V/17.0)+2.0373e-1*exp(-V/150))
IC2→IF, C2→C1	α12= 8.5539/(7.4392e-2*exp(-V/15.0)+ 2.0373e-1*exp(-V/150))
C1→O	α13= 8.5539/(7.4392e-2*exp(-V/12.0)+ 2.0373e-1*exp(-V/150))
IC2→IC3, C2→C3	β11= 7.5215e-2*exp(-V/20.3)
IF→IC2, C1→C2	β12= 2.7574*exp(-(V-5)/20.3)
O→C1	β13= 4.7755e-1*exp(-(V-10)/20.3)
IC3→C3, IC2→C2, IF→C1	α3=5.1458e-6*exp(-V/8.2471)
C3→IC3, C2→IC2, C1→IF	β3=6.1205*exp(V/12.542)
O→IF	α2= 13.370*exp(V/43.749)
IF→O	β2= (α13* α2* α3)/(β13* β3)
O→IS	αx= 3.4229e-2*α2
IS→O	βx= 1.7898e-2*α3
C3, C2, C1, O → BC3, BC2, BC1, BO	μ1 = 2.0462e-7 (WT); 2.7252e-7 (HF)
BC3, BC2, BC1, BO → C3, C2, C1,O	μ2 = 8.9731e-4 (WT); 1.9701e-4 (HF)

Optimization procedure for ΔKPQ mutant sodium channel

Five pacing protocols were optimized: steady state availability [3] (shown to be similar to WT [4]), steady state activation [5] (shown to be similar to WT [4]), recovery from inactivation at -90mV [6], recovery from use-dependent block at -100mV, and time constant of inactivation from the open state [6]. The model was further constrained by channel mean open time [4].

A cost function for each protocol was defined as the sum of squared differences between experiment and simulation. The total cost function (sum of the individual protocol errors) was then minimized and converged when a tolerance of 0.01 for the change of the cost function and 0.01 for the change in parameters was achieved. The initial conditions were set as the optimized WT Na^+ channel recently published [1]. For the aforementioned protocols, entry and egress from the bursting state (μ1 and μ2, respectively) were set at 0 (no bursting during optimization).

After initial optimization, bursting states were added to the model [7], and denoted with the prefix *B* (***B***C3, ***B***C2, ***B***C1, ***B***O), as described for wild-type. The rate constants of the bursting regime (μ1, μ2) were then optimized (all other rate constants held constant) to yield a sustained inward current of either 0.5% (O'Hara-Rudy model [8]) or 1% (ten Tusscher [9] or Grandi-Bers model [10]) of the peak Na^+ current [4, 11] at tonic pacing (BCL = 3000).

Online Table II

Transition rates ΔKPQ Mutant Na^+ channel (ms^{-1})	
IC3 →IC2, C3→C2, BC3→BC2	α11= 1.6662e+01 /(6.7574e-02*exp(-V/17.0)+8.0935e-02*exp(-V/150))
IC2→IF, C2→C1, BC2→BC1	α12= 1.6662e+01 /(6.7574e-02*exp(-V/17.0)+8.0935e-02*exp(-V/150))
C1→O, BC1→BO	α13= 1.6662e+01 /(6.7574e-02*exp(-V/17.0)+8.0935e-02*exp(-V/150))
IC2→IC3, C2→C3, BC2→BC3	β11= 1.4984e-01*exp(-V/20.3)
IF→IC2, C1→C2, BC1→BC2	β12= 1.0868e+01*exp(-(V-5)/20.3)
O→C1, BO→BC1	β13= 1.9349e-01*exp(-(V-10)/20.3)
IC3→C3, IC2→C2, IF→C1	α3=2.6699e-6*exp(-V/7.5168)
C3→IC3, C2→IC2, C1→IF	β3=1.7538e+01*exp(V/11.010)
O→IF	α2= 7.6104*exp(V/214.37)
IF→O	β2= (α13* α2* α3)/(β13* β3)
O→IS	αx= 8.6589e-02*α2
IS→O	βx= 1.4265e-02*α3
C3→BC3, C2→BC2, C1→BC1, O→BO	μ1 = 1.4397e-6 (0.5% late); 2.6589e-06 (1% late)
BC3→C3, BC2→C2, BC1→C1, BO→O	μ2 = 5.6593e-4 (0.5% late); 4.6274e-04 (1% late)

Optimization procedure for the drug channel interaction

Online Table III: Situation-Dependent Affinities of Ranolazine to the WT and ΔKPQ Na^+ Channel (Experimental Data)

	WT	**ΔKPQ**
Tonic Block of Late I_{Na}	6 μM [12]	12.66 μM, n = 0.7301 *
I_{Kr}	12 μM [13]	12 μM [13]
Tonic Block of Peak I_{Na}	165.2 μM, n = 1.623 *	120.8 μM, n = 1.115 *
Use-Dependent Block of I_{Na}	100.5 μM, n = 1.015 *	83.11 μM, n = 0.9082 *

n = Hill coefficient
* Kass laboratory

The Na^+ drug-channel model parameters for the on and off rates of ranolazine are taken from experiments where available. These include diffusion rates that indicate drug on rates "k_{on}" = [drug]* D (diffusion rate) and affinities (Kd) to discrete conformations that determine drug off rates "k_{off}" = Kd*D (diffusion rate). The diffusion rate for ranolazine was assumed similar to other local anesthetics [14, 15], and set at 5500 $M^{-1}ms^{-1}$ in the computational model. Rates were also constrained by experimental data (described in detail below) and microscopic reversibility as in Colquhoun [16].

Optimization of Wild-Type and Ranolazine Model

Five experimental protocols were used to constrain the model: steady state availability (SSA), tonic block (TB) of peak and late current, use-dependent block (UDB), recovery from UDB (RUDB), and frequency-dependent UDB (FDUDB). Charged drug rate constants (ax1, bx1, a13c, a22, b33, a33, $Kd_{0,Bursting}$), and neutral drug rate constants (ax2, a13n, a_22, b_33) were optimized.

Open state affinity for the charged form of ranolazine was derived from the Kd value from use-dependent block (UDB), and assumed to measure affinity to the open state. 100.5 μM was set as Kd_0 – the Kd at 0 mV. Closed state affinity of charged drug was then calculated using Eyring rate theory for the voltage dependence of rate constants ($Kd= Kd_0*e^{(-d*V*F/(R*T))}$) [17]. For example, the computed Kd value at -100 mV for charged ranolazine is computed to be 1578 μM.

Bursting state affinity for charged ranolazine was initially set at the value found by assuming the affinity of tonic block of late I_{Na} was equal to Kd at -100 mV. Using $Kd= Kd_0*e^{(-d*V*F/(R*T))}$, Kd_0 was then calculated and used as an initial value in the optimization. For example, the affinity of TB $I_{Na,L}$ for WT is 6 μM [12]; if that value is assumed to equal Kd_{-100mV}, $Kd_{0,Bursting}$ was initially set at 0.3822 μM.

Affinities of the neutral fraction of ranolazine to drug-bound states ($Kd_{neutral}$, $Kd_{inactive\_neutral}$, $Kd_{closed\_neutral}$) were initially held constant and assumed similar to flecainide [1, 18]; because the model gave acceptable fits to the data, those rates were kept. The optimized rate constants are shown in the table below.

Optimization of ΔKPQ and Ranolazine Model

Four experimental protocols were used to constrain the model: tonic block (TB) of peak and late current, use-dependent block (UDB), recovery from UDB (RUDB), and frequency-dependent UDB (FDUDB). Charged drug rate constants (ax1, bx1, a13c, a22, b33, a33, $Kd_{0,Bursting}$), and neutral drug rate constants (ax2, a13n, a_22, b_33, $Kd_{neutral}$, $Kd_{inactive\_neutral}$, $Kd_{closed\_neutral}$) were optimized.

Open state affinity of the charged form of ranolazine was derived from the Kd value from use-dependent block (UDB), as described above for WT, and set at 83.11 μM. Closed state affinity of charged drug was then calculated using Eyring rate theory for the voltage dependence of rate constants ($Kd= Kd_0*e^{(-d*V*F/(R*T))}$) [17]. Bursting state affinity for charged ranolazine was initially set at the value found by assuming the affinity of tonic block of late I_{Na} was equal to Kd at -100 mV, as described above for WT, and $Kd_{0,Burst}$ was initially set at 0.8064 μM.

Affinities of the neutral fraction of ranolazine to drug-bound states ($Kd_{neutral}$, $Kd_{inactive\_neutral}$, $Kd_{closed\_neutral}$) were initially set to flecainide [1, 18], but were allowed to change throughout the optimization. The optimized rate constants are shown in the table below.

Online Table IV

WT Ranolazine	
Transition rates (ms^{-1})	
$k_{on} = k_{closed, on}$	[D+]*Diffusion
$k_{off} = k_{closed, off}$	$k_{d, open}$ *Diffusion ; (kd_{open}= 100.5e-6*exp(-0.7*V*F/R*T))
$k_{bursting, on} = k_{closed\ bursting, on}$	[D+]*Diffusion
$k_{bursting, off} = k_{closed\ bursting, off}$	$kd_{Bursting,Open}$ *Diffusion ; ($kd_{Bursting,Open}$ = 1.5012e-6*exp(-0.7*V*F/R*T))
$k_{neutral, on}$	[D]*Diffusion
$k_{neutral, off}$	400e-6*Diffusion
$k_{neutral, inactivated, on}$	$k_{neutral, on}$
$k_{neutral, inactivated, off}$	5.4e-6*Diffusion
$k_{neutral, closed, on}$	$k_{neutral, on}$
$k_{neutral, closed, off}$	800e-6*Diffusion
$D^+IC3 \rightarrow D^+IC2$, $D^+C3 \rightarrow D^+C2$, DIC3 →DIC2, DC3→DC2	α11
$D^+IC2 \rightarrow D^+IF$, $D^+C2 \rightarrow D^+C1$, DIC2→DIF, DC2→DC1	α12
$D^+IC2 \rightarrow D^+IC3$, $D^+C2 \rightarrow D^+C3$, DIC2→DIC3, DC2→DC3	β11
$D^+IF \rightarrow D^+IC2$, $D^+C1 \rightarrow D^+C2$, DIF→DIC2, DC1→DC2	β12
$D^+O \rightarrow D^+IS$	αx1 = 4.4923e+3 *αx
$D^+IS \rightarrow D^+O$	βx1 = 2.7031e-01 *βx
DO→DIS	αx2 = 1.4947e+01 *αx
$D^+C1 \rightarrow D^+O$	α13c = 3.6811*a13
DC1→DO	α13n = 2.3570e+02*α13
$D^+O \rightarrow D^+C1$	b13c = (β13*kcon*koff*α13c)/(kon*kcoff*α13)
DO→DC1	b13n = (β13*kc_on*α13n*k_off)/(kc_off*α13*k_on)
DIS→DO	βx2 = (βx*k_on* αx2*ki_off)/(αx*ki_on*k_off)
$D^+O \rightarrow D^+IF$	α22 = 6.8705e+04 *α2
DO→DIF	α_22 = 2.1182e+02 *α2
$D^+IF \rightarrow D^+O$	β22 = (α13c* α22* α33)/(β13c* β33)
DIF→DO	β_22 = (α_33*α13n*α_22)/(β_33*β13n)
$D^+C3 \rightarrow D^+IC3$, $D^+C2 \rightarrow D^+IC2$, $D^+C1 \rightarrow D^+IF$	β33 = 1.7561e-01 *β3
DC3→DIC3, DC2→DIC2, DC1→DIF	β_33 = 1.2197e-03*β3
$D^+IC3 \rightarrow D^+C3$, $D^+IC2 \rightarrow D^+C2$, $D^+IF \rightarrow D^+C1$	α33 = 4.0832e-02 *α3
DIC3→DC3, DIC2→DC2, DIF→DC1	α_33 = (ki_off* α3*kc_on* β_33)/(ki_on*kc_off* β3)
Diffusion	5500 $M^{-1}ms^{-1}$

Online Table V

ΔKPQ Ranolazine	
Transition rates (ms^{-1})	
$k_{on} = k_{closed, on}$	[D+]*Diffusion
$k_{off} = k_{closed, off}$	$k_{d, open}$ *Diffusion ; (kd_{open}= 83.11e-6*exp(-0.7*V*F/R*T))
$k_{bursting, on} = k_{closed\ bursting, on}$	[D+]*Diffusion
$k_{bursting, off} = k_{closed\ bursting, off}$	$kd_{Bursting,Open}$ *Diffusion ; ($kd_{Bursting,Open}$ = 3.8367e-6*exp(-0.7*V*F/R*T))
$k_{neutral, on}$	[D]*Diffusion
$k_{neutral, off}$	2.6479e+02e-6*Diffusion
$k_{neutral, inactivated, on}$	$k_{neutral, on}$;
$k_{neutral, inactivated, off}$	19.034e-6*Diffusion
$k_{neutral, closed, on}$	$k_{neutral, on}$;
$k_{neutral, closed, off}$	61.842e-6*Diffusion
$D^+IC3 \rightarrow D^+IC2$, $D^+C3 \rightarrow D^+C2$, DIC3 →DIC2, DC3→DC2	α11
$D^+IC2 \rightarrow D^+IF$, $D^+C2 \rightarrow D^+C1$, DIC2→DIF, DC2→DC1	α12
$D^+IC2 \rightarrow D^+IC3$, $D^+C2 \rightarrow D^+C3$, DIC2→DIC3, DC2→DC3	β11
$D^+IF \rightarrow D^+IC2$, $D^+C1 \rightarrow D^+C2$, DIF→DIC2, DC1→DC2	β12
$D^+O \rightarrow D^+IS$	αx1 = 3.0028e-01*αx
$D^+IS \rightarrow D^+O$	βx1 = 2.1775e-02*βx
DO→DIS	αx2 = 3.8814e-02*αx
$D^+C1 \rightarrow D^+O$	α13c = 4.7577e-01*α13
DC1→DO	α13n = 3.3694e+01*α13
$D^+O \rightarrow D^+C1$	b13c = (β13*kcon*koff*α13c)/(kon*kcoff*α13)
DO→DC1	b13n = (β13*kc_on*α13n*k_off)/(kc_off*α13*k_on)
DIS→DO	βx2 = (βx*k_on* αx2*ki_off)/(αx*ki_on*k_off)
$D^+O \rightarrow D^+IF$	α22 = 8.9205e+01*α2
DO→DIF	α_22 = 4.3865e-02*α2
$D^+IF \rightarrow D^+O$	β22 = (α13c* α22* α33)/(β13c* β33)
DIF→DO	β_22 = (α_33*α13n*α_22)/(β_33*β13n)
$D^+C3 \rightarrow D^+IC3$, $D^+C2 \rightarrow D^+IC2$, $D^+C1 \rightarrow D^+IF$	β33 = 3.4549e-04*β3
DC3→DIC3, DC2→DIC2, DC1→DIF	β_33 = 4.2894*β3
$D^+IC3 \rightarrow D^+C3$, $D^+IC2 \rightarrow D^+C2$, $D^+IF \rightarrow D^+C1$	α33 = 2.9425e-02*α3
DIC3→DC3, DIC2→DC2, DIF→DC1	α_33= (ki_off* α3*kc_on* β_33)/(ki_on*kc_off* β3)
Diffusion	5500 $M^{-1}ms^{-1}$

Simulation of I_{Kr} Blockade

To simulate the effects of ranolazine on I_{Kr} current, we decreased the peak conductance, G_{IKr} in a concentration dependent fashion using a concentration response relationship with a Hill coefficient of 1 (n = 1) as follows:

$$G_{IKr} = G_{IKr,\max} * \left(\frac{1}{1 + (Drug / IC_{50})^n} \right)$$

where $G_{IKr,max}$ is the nominal conductance value from the given human ventricular myocyte model used (O'Hara-Rudy [8], ten Tusscher [9], or Grandi-Bers [10]) and IC_{50} is the concentration of drug that produces a 50% inhibition of I_{Kr} current.

Cellular simulations

The model formulation for virtual (O'Hara-Rudy [8], ten Tusscher [9], or Grandi-Bers [10] with Soltis-Saucerman model [19]) epicardial cells was used with the published Na^+ channel replaced with the model described here. State probabilities in the Markov model of the Na^+ channel were computed by an implicit Trapezoidal numerical method. The numerical method for updating the voltage was forward Euler.

The Soltis-Saucerman model of CaMKII and PKA signaling pathways [19] was merged with the Grandi-Bers human model [10]. We used the Soltis-Saucerman model as a template to replace each ionic current with the Grandi-Bers model except for the L-type calcium channels (LTCC, the seven-state Markov model). We then adjusted the Ca^{2+} current amplitude in the Grand-Bers model to match current experimental human data [20] and G_{Kr} was increased by 3 fold. We also replaced the nominal Na^+ channel model with our Na^+ drug-channel models as described above. Isoproterenol was set to 0 in mutant simulations (Figure 4).

For the O'Hara-Rudy ΔKPQ model, we made a heterozygote mutant (50% mutant Na^+ channels, 50% WT Na^+ channels), and included 0.5% late Na^+ current, as this model easily produced EADs and exhibited repolarization failure with 1% late Na^+ current. For the ten Tusscher ΔKPQ model, we made a heterozygote with 1% late Na^+ current. The Grand-Bers ΔKPQ model was a heterozygote with 1% late Na^+ current.

One-dimensional simulations

One-dimensional simulations were modified with experimental transmural data from [21] which show a linear decrease in APD from endocardium to epicardium. The maximal conductance G_{Ks} was monotonically increased from 0.15 at the endocardium (cell 1) to 0.30 at the epicardium (cell 165). Cells 1 – 40 were endocaridal, and cells 41 – 165 were epicardial, and utilized the nominal values of G_{to} of ten Tusscher [9]. These ionic conductances gave an endocaridal APD of 379 ms, an epicaridal APD of 335 ms, and a QTc of 391.75 ms (at 1Hz pacing), consistent with experimental optical imaging data [21, 22]. For O'Hara-Rudy [8] and Grandi-Bers [10] model without β–adrenergic stimulation, the maximal conductance G_{Kr} was monotonically increased from 0.046 and 0.03 at the endocardium (cell 1) to 0.0598 and 0.035 at the epicardium (cell 165), respectively. Cells 1 – 40 were endocaridal, and cells 41 – 165 were epicardial. These ionic conductances gave an endocaridal APD of 268 ms in O'Hara and 355 ms in Grandi model, an epicaridal APD of 212 ms in O'Hara and 330 ms in Grandi model, and a QTc of 300 ms in O'Hara and 360 ms in Grandi model (at 1Hz pacing).

A 165-cell cable was unstimulated for 10 minutes without drug. Drug was then "applied" and cells paced (-250 pA/pF for 1 ms) for 500 beats at a given pacing cycle length and drug concentration. The numerical method was forward Euler.

Pseudo ECG computation

Extracellular unipolar potentials (ϕ_E) generated by the fiber in an extensive medium of conductivity σ_e, were computed from the transmembrane potential V_m using the integral expression as in Plonsey and Barr [23] and Gima and Rudy [24]:

$$\Phi_E(x',y',z') = \frac{a^2\sigma_i}{4\sigma_e}\int(-\nabla V_m)\cdot\left[\nabla\frac{1}{r}\right]dx$$

$$r = \left[(x-x')^2+(y-y')^2+(z-z')^2\right]^{1/2}$$

where ∇V_m is the spatial gradient of V_m, a is the radius of the fiber, σ_i is the intracellular conductivity, and r is the distance from a source point (x, y, or, z) to a field point (x', y', or, z'). Φ_E was computed at an electrode site 2.0 cm away from the distal end along the fiber axis [25].

Cell Expression and Electrophysiology of the ΔKPQ mutation

Site-directed mutagenesis was done on $Na_V1.5$ in pcDNA3.1 using the Quik Change site-directed mutagenesis kit (Stratagene). Whole cell recordings were made on Human Embryonic Kidney (HEK) 293 cells expressing WT and mutant $Na_V1.5$ channels along with hβ1 subunits (Lipofectamine, Invitrogen).

Patch clamp procedures were used with the following internal solution (in mM): 50 aspartic acid, 60 CsCl, 5 Na2ATP, 11 EGTA, 10 HEPES, 4.27 CaCl2 (resulting in a final $[Ca^{2+}]i$ of 100 nM), and 1 $MgCl_2$, pH 7.4 adjusted with CsOH. The external solutions for measurement of all Na^+ channel activity contained (in mM): 130 NaCl, 2 $CaCl_2$, 5 CsCl, 1.2 $MgCl_2$, 10 HEPES, and 5 glucose, pH 7.4 adjusted with NaOH.

TTX was purchased from Ascent Scientific (UK). Ranolazine was purchased from Sigma Aldrich (St. Louis, MO). Drugs were applied locally to the outside of the cell being patched via homemade perfusion system using microfluidic valves (Lee Co, Essex, CT). Currents were measured at room temperature (~23 °C). Pipettes were borosilicate from VWR (West Chester, PA). Typical pipette resistance was between 1.5 and 3 MΩ. After whole cell configuration is achieved only cells with access resistance less than 7 MΩ are recorded. Membrane currents were measured with Axopatch 200B amplifiers (Axon Instruments, Foster City, CA). Capacitance and series resistance compensation were carried out using analog techniques according to the amplifier manufacturer (Axon Instruments, Foster City, CA). Only cells with access resistance and peak current that, after compensation, have voltage errors less than 5 mV are used for analysis. PClamp8 (Axon Instruments) was used for data acquisition and initial analysis. Analysis was carried out in Excel (Microsoft), Origin 7.0 (Microcal Software, Northampton, MA), and programs written in Matlab (The Mathworks, Natick, MA). Analyzed data are shown as mean +/− S.E.M. Statistical significance was tested using Student's t test; $p < 0.05$ was considered statistically significant.

Simulation of human heart failure

Cell model

The Grandi-Bers model with Soltis-Saucerman β-adrenergic signaling pathway (see above) was used for heart failure simulations. The epicardial cell was paced to 1060 seconds with 2 Hz pacing (BCL 500), and spontaneous activity was observed after stimulus removal.

CaMKII and PKA regulation

For the CaMKII and PKA phosphorylation, we added the regulation on I_{Ks}, LTCC and RyR as in Soltis-Saucerman [19], highlighting the following regulatory pathways: (1) I_{Ks} is regulated by PKA phosphorylation; (2) I_{CaL} and RyR opening are modulated by CaMKII and PKA; (3) RyR leak is CaMKII dependent; (4) CaMKII and PKA phosphorylate PLB that alternate SERCA fluxes; (5) the cystic fibrosis transmembrane conductance regulator Cl^- current regulated by PKA, and (6) Troponin I (TnI) is regulated by PKA. Here we also included (7) the effect of PKA to phosphorylate PLM and increase NKA activity in the model [26].

Current density changes in heart failure

To simulate human heart failure (HF), we modified the current density changes in HF shown in Online Table VI, below. In addition, CaMKII expression is increased in failing human myocardium [27]. We simulated CaMKII overexpression (CaMKII-OE) as in Soltis-Saucerman [19]: (1) Increased $I_{to,slow}$ amplitude and I_{to} recovery from inactivation by CaMKII-OE (See [19] for detailed equations); and (2) CAMKII-OE effects has been shown to shift I_{Na} to the hyperpolarizing direction, delay recovery from inactivation. To simulated CaMKII-OE effects alterations to I_{Na}: rate constant $\beta 3$ was increased by 2.4-fold.

Online Table VI: Current density changes induced in the failing heart

Ionic current	Percentage Change	Species	References
$\mathbf{I_{NaL}}$	10x *increase* (0.1% → 1%)	Human	28
$\mathbf{I_{to,fast}}$	36% *decrease*	Human	29
$\mathbf{I_{K1}}$	25% *decrease*	Human	30, 31
SERCA	36% *decrease*	Human	32
$\mathbf{k_{leak}}$ **(SR leak)**	3.5-fold *increase*	Rabbit	33
$\mathbf{I_{Na,\ leak}}$ *	16-fold *increase*	Rabbit	34
$\mathbf{I_{NaK}}$ **(Na^+/K^+-ATPase)***	10 - 42% *decrease*	Human	35-37

*Note: Models of modified I_{NaK} and $I_{Na,\ background}$ currents are set within the range of experimental data and parameter space is analyzed in Figures 7 and 8.

SR – sacrcoplasmic reticulum

Simulation of the drug interaction with Na^+ leak current ($I_{Na,Leak}$)

To simulate the effects of drugs on Na^+ leak current during heart failure, we decreased the peak conductance of $I_{Na,Leak}$ in a concentration-dependent manner using a concentration response relationship with a Hill coefficient (n) as follows:

$$G_{Na,Leak} = G_{Na,Leak,\max} * \left(\frac{1}{1 + (Drug / IC_{50})^n} \right)$$

where $G_{Na,Leak,max}$ is the nominal conductance from the Grandi model, and IC_{50} corresponds to the sensitivity of the channels to ranolazine assuming peak current affinity (165.2 μM, n = 1.6), or late current affinity (6 μM, n = 1) [12]. In Online Figure VII and VIII, we assume peak current affinity, and in Figure 7, 8, Online Figure V and VI, we assume late current affinity.

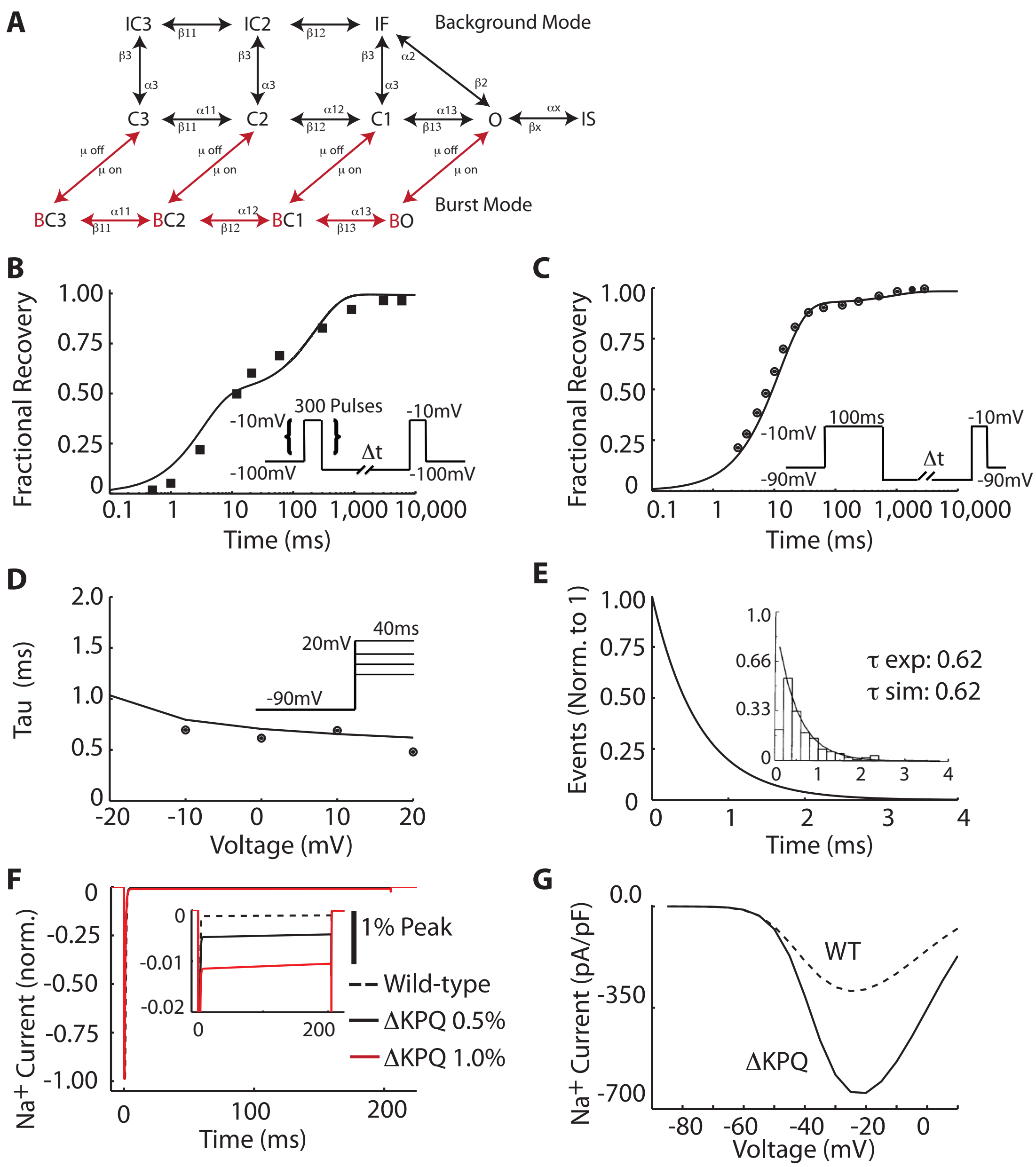

Online Figure I: ΔKPQ mutant Na^{+} channel kinetics.

(A) Schematic of the bursting states. In B – D, the points are experiment, lines are simulation. (B) Recovery from UDB induced by trains of 100 pulses (-10 mV for 25 ms at 25 Hz) from -100 mV in drug free conditions. Test pulses (-10 mV) were after variable recovery intervals at -100 mV. Currents were normalized to tonic block. (C) Recovery from inactivation induced by a depolarizing pulse (-10 mV for 100 ms) from -90 mV. Test pulses (-10 mV) were after variable recovery intervals at -90 mV [6]. (D) Time constant of inactivation, induced from a holding potential of -100 mV to indicated voltages [4]. (E) Mean open time at -30 mV [4]. (F) Optimization of entry and egress from the bursting mode (μ_1 and μ_2 respectively) to induce a 0.5% (black) or 1% (red) persistent inward Na^{+} current. (G) Current – voltage relationship indicating ΔKPQ has nearly double current density as compared to WT [4].

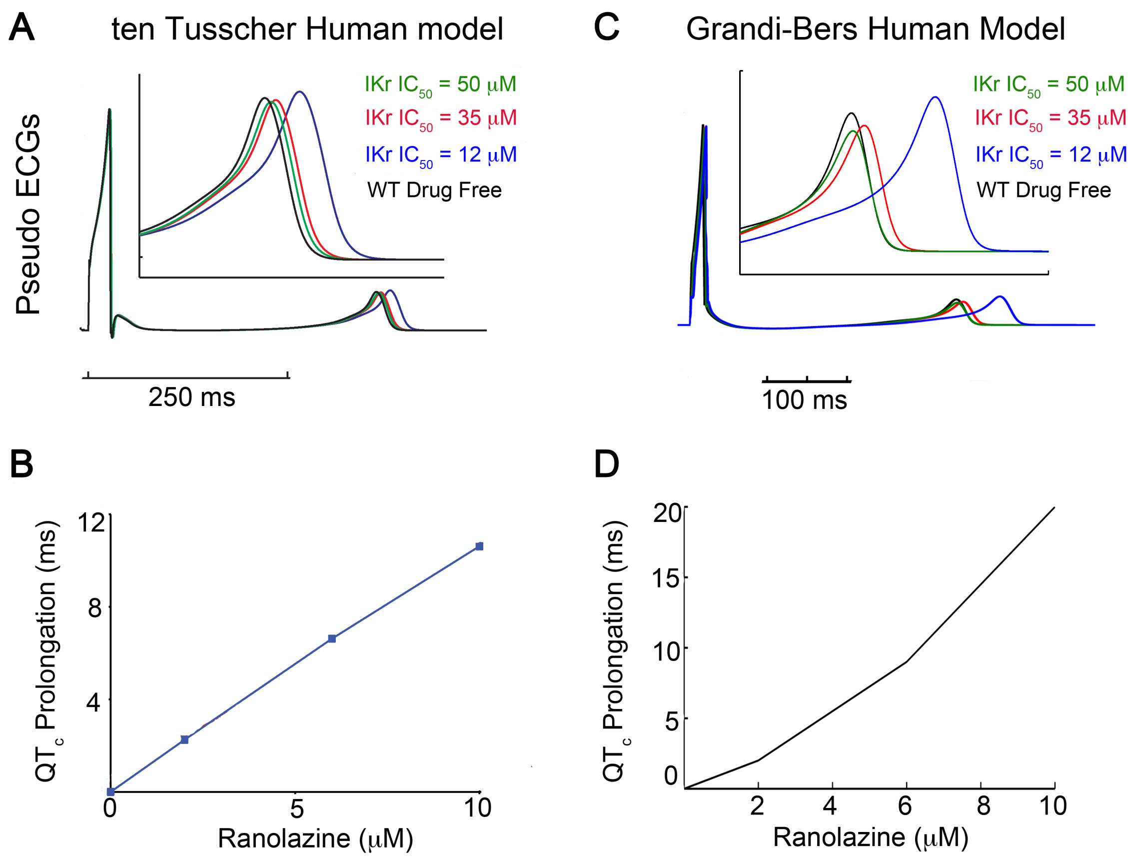

Online Figure II: Consideration of ranolazine metabolites for I_{Kr} inhibition predicts clinical QTc prolongation.

Shown in (A) are computed ECGs of a 165-cell cardiac fiber with 6 μM ranolazine (therapeutic concentration), and varying values for IC_{50} of I_{Kr} inhibition (see **Supplementary Information**). I_{Kr} inhibition at IC_{50} = 50 μM (green) produces a 2.5 ms QTc prolongation; I_{Kr} inhibition at IC_{50} = 12 μM (blue) prolongs QTc by 20.3 ms; I_{Kr} inhibition at IC_{50} = 35 μM (red) prolongs QTc by 5.45 ms. (B) Concentration-dependent ΔQTc is approximately linear over the therapeutic range of ranolazine. See text for details. (C) and (D) are for the Grandi-Bers human model: QT prolongation with IC_{50} = 12 μM, 35 μM, and 50 μM are 59 ms, 8 ms, and 1 ms, respectively.

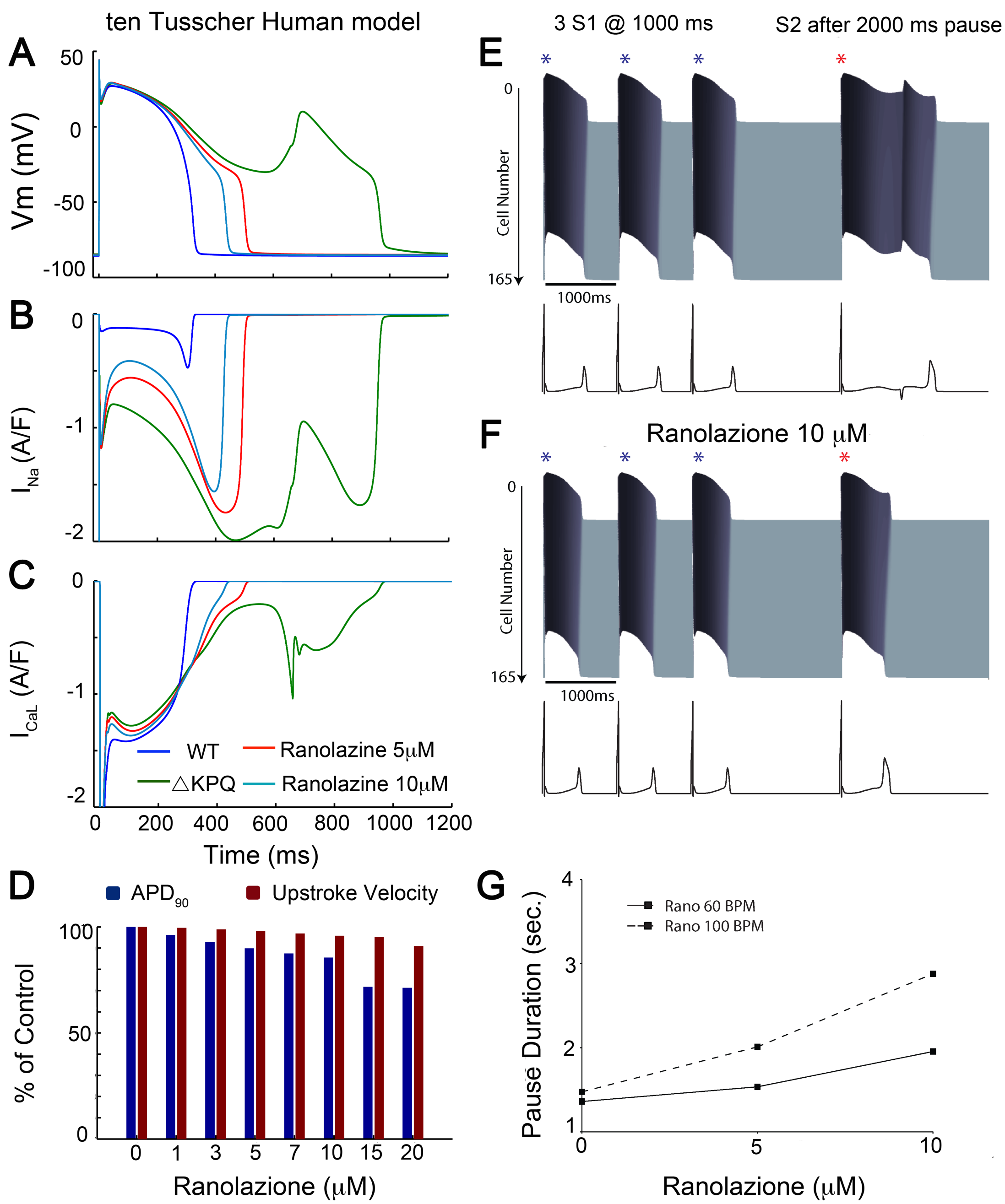

Online Figure III: Effects of a pause on incident EADs generated in the subsequent beat for the ten Tusscher human ventricular myocyte model.
The effects of the ΔKPQ mutation are shown for the ten Tusscher human ventricular myocyte model, and yields qualitatively similar results to the O'Hara Rudy and the Grandi-Bers models shown in Figure 4. Panel (A) depicts cellular APs, (B) depicts Na^+ currents (peak off scale), and (C) depicts the L-type Ca^{2+} currents (peak off scale). In all three models, low (5 μM), and high (10 μM) ranolazine progressively shortens the APD but fails to fully normalize to WT (blue line). Panel (D) depicts concentration dependent effects of ranolazine on action potential duration (APD) and upstroke velocity (UV) at BCL 1000. A comparison to Figure 4 reveals that the O'Hara Rudy and Grandi-Bers models are much more effective at normalizing the APD in the

highest concentrations tested. For all three models, UV remains robust with high therapeutic concentrations of drug. Panels (E-G) are the tissue level simulations. Panel (E) shows a space-time plot of 3 S1 beats at BCL1000 (after steady state pacing – 500 beats) in the absence of drug. A 2000 ms pause, followed by an S2 stimulus elicits an EAD throughout the 165-cell cardiac fiber. With pretreatment of 10 μM ranolazine (F), the S2 stimulus fails to elicit an EAD throughout the fiber and monotonic repolarization is restored. For (E) and (F), x-axis is time, y-axis is cell number, z-axis is voltage. A computed ECG is underneath the space-time plot. (G) The pause necessary to elicit an EAD throughout a 165-cell cardiac fiber with assessed in 5 ms increments for two pacing cycles (60 BPM – solid line, 100 BPM – dotted line) with 10 μM ranolazine after steady state pacing at the given cycle length (500 beats).

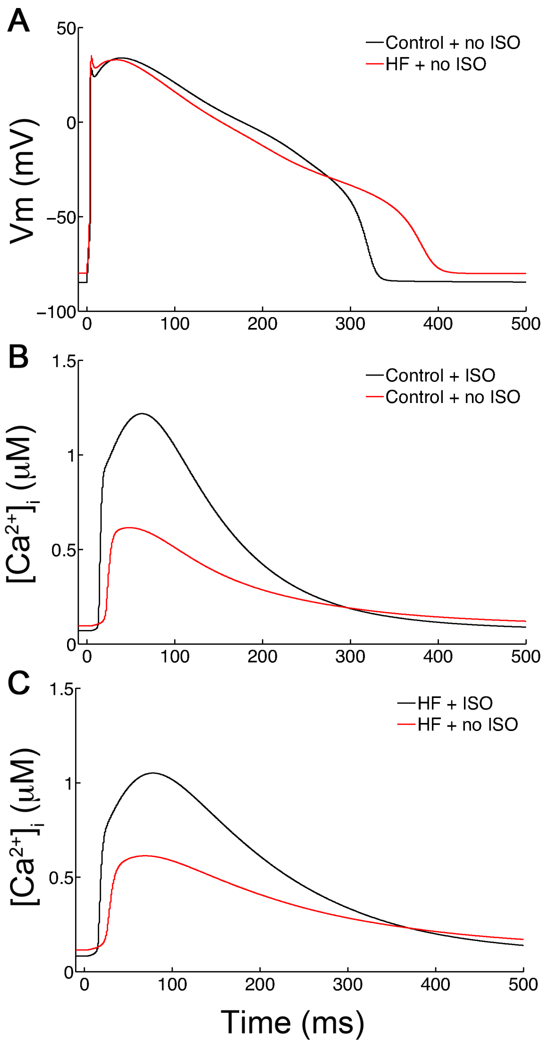

Online Figure IV: Comparison of Ca^{2+} transient in control and HF conditions
Shown in (A) are cellular APs in the control (black) and heart failure (HF condition same as in Figure 6 - red) at BCL 1000 ms without β–adrenergic stimulation. (B) Intracellular Na^+ concentration with 1 μM (black) and 0 μM isoproterenol applications (red) in control case. (C) In the heart failure model, intracellular Na^+ concentration with 1 μM (black) and 0 μM isoproterenol applications (red) in control case.

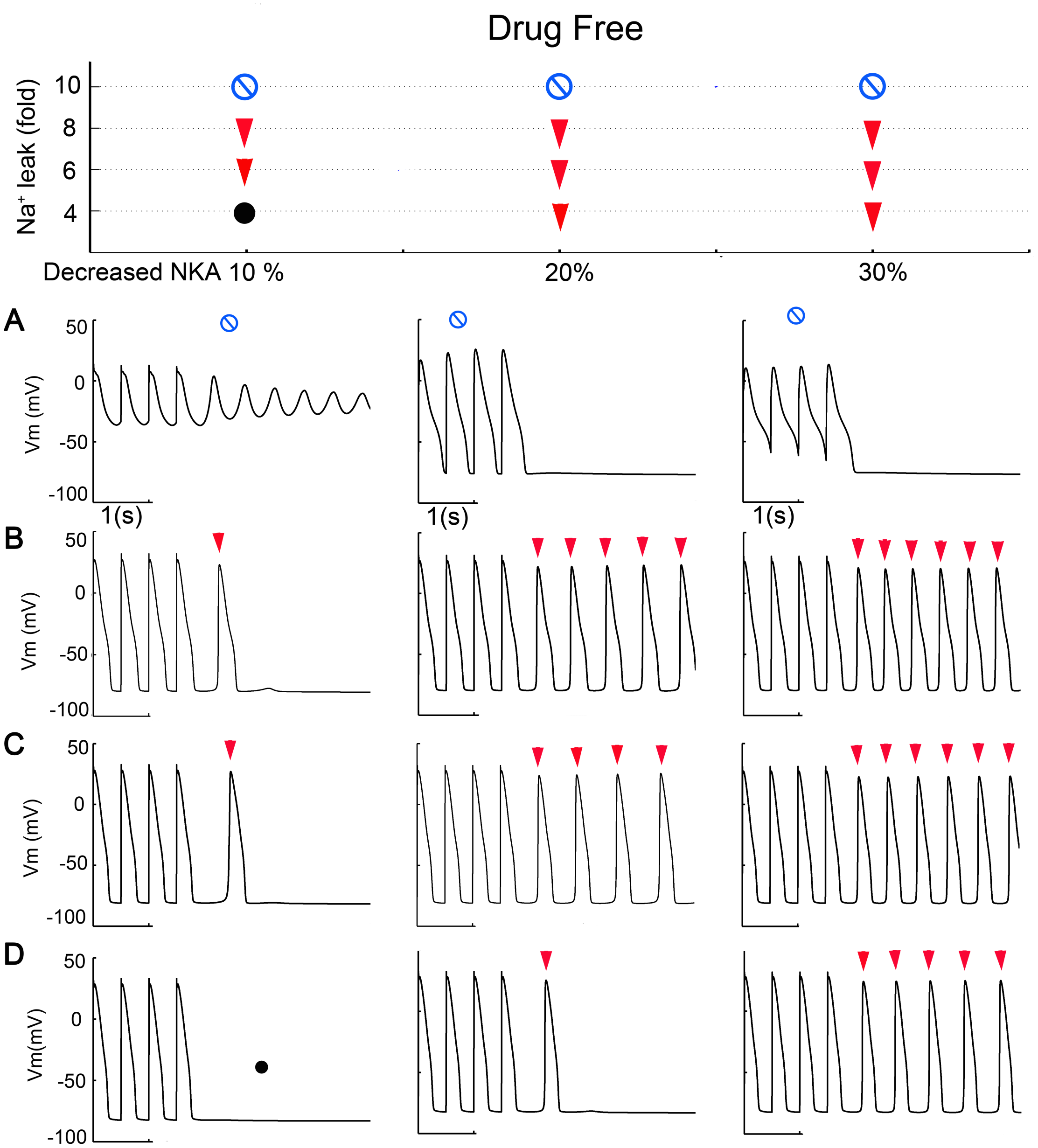

Online Figure V: Summary data of DAD formation in the drug-free conditions of Figure 7. Action potentials shown for each condition in Figure 7, drug free. Row (A) indicates 10-fold Na^+ leak, (B) indicates 8-fold Na^+ leak, (C) indicates 6-fold Na^+ leak, and (D) indicates 4-fold Na^+ leak. Column 1 corresponds to 10% decreased NKA, column 2 is 20% decrease, and column 3 is 30% decrease. As in Figure 7, filled circles indicate absence of DADs, upside-down red triangles indicate presence of DADs, and stop signs (⃠) indicate repolarization failure.

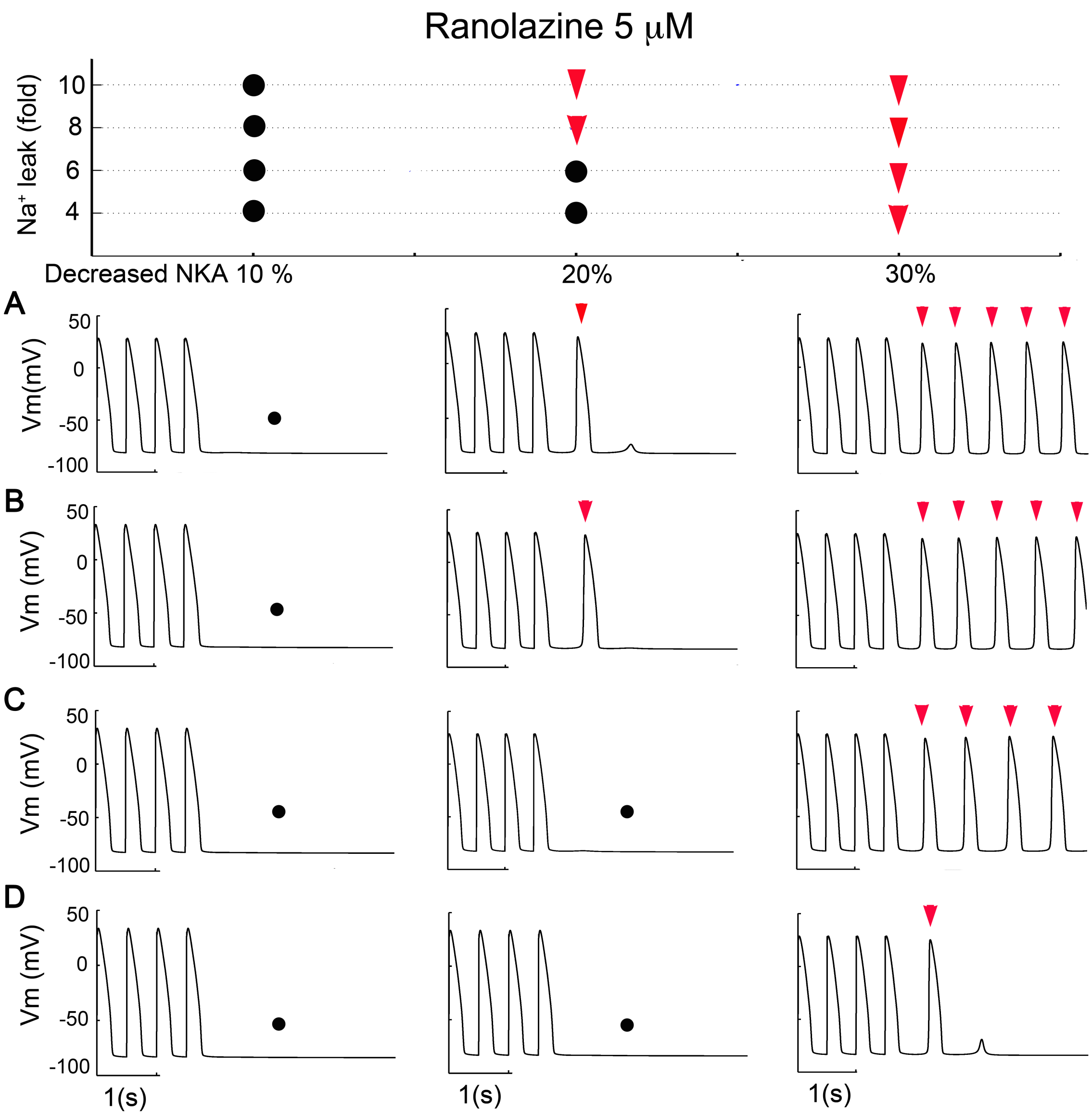

Online Figure VI: DAD abolishment with ranolazine 5 μM when Na^+ leak current is sensitive at an affinity equivalent to late Na^+ current blockade.

Summary data and expanded AP waveforms assuming that ranolazine affinity is equivalent to late current affinity (IC_{50} = 6 μM – Figure 7). Row (A) indicates 10-fold Na^+ leak, (B) indicates 8-fold Na^+ leak, (C) indicates 6-fold Na^+ leak, and (D) indicates 4-fold Na^+ leak. Column 1 corresponds to 10% decreased NKA, column 2 is 20% decrease, and column 3 is 30% decrease. Filled black circles (•) indicate absence of DADs, upside down red triangles indicate presence of DADs. See **Supplementary Information** for details on calculation of Na^+ leak current blockade.

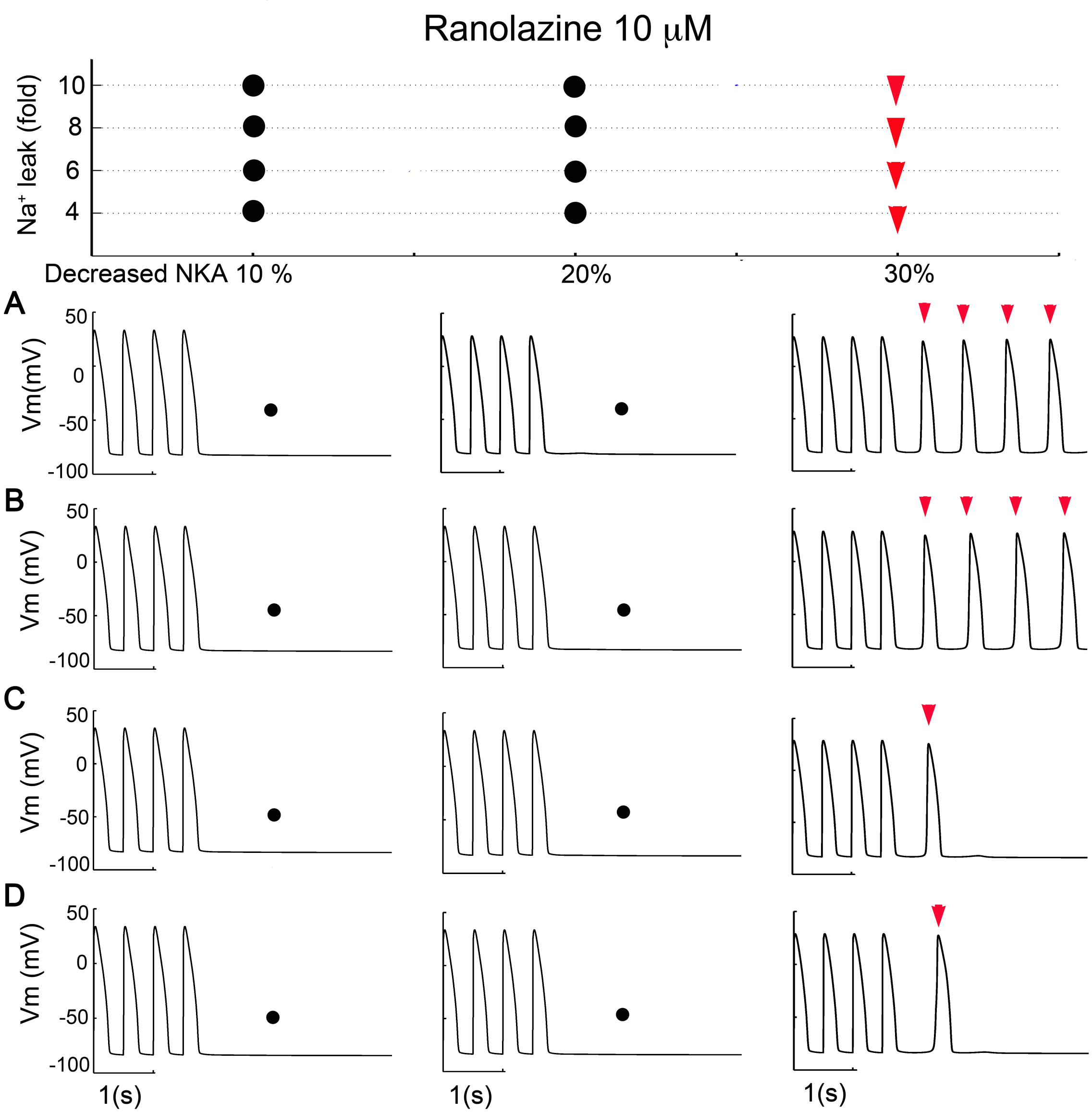

Online Figure VII: DAD abolishment with ranolazine 10 μM when Na^+ leak current is sensitive at an affinity equivalent to late Na^+ current blockade.

Summary data and expanded AP waveforms assuming that ranolazine affinity is equivalent to late current affinity (IC_{50} = 6 μM – Figure 7). Row (A) indicates 10-fold Na^+ leak, (B) indicates 8-fold Na^+ leak, (C) indicates 6-fold Na^+ leak, and (D) indicates 4-fold Na^+ leak. Column 1 corresponds to 10% decreased NKA, column 2 is 20% decrease, and column 3 is 30% decrease. As expected, with ranolazine 10 μM, more DADs are abolished, compared to low-dose drug (Figure 7 and Online figure 5). Filled black circles (•) indicate absence of DADs, upside down red triangles indicate presence of DADs. See **Supplementary Information** for details on calculation of Na^+ leak current blockade.

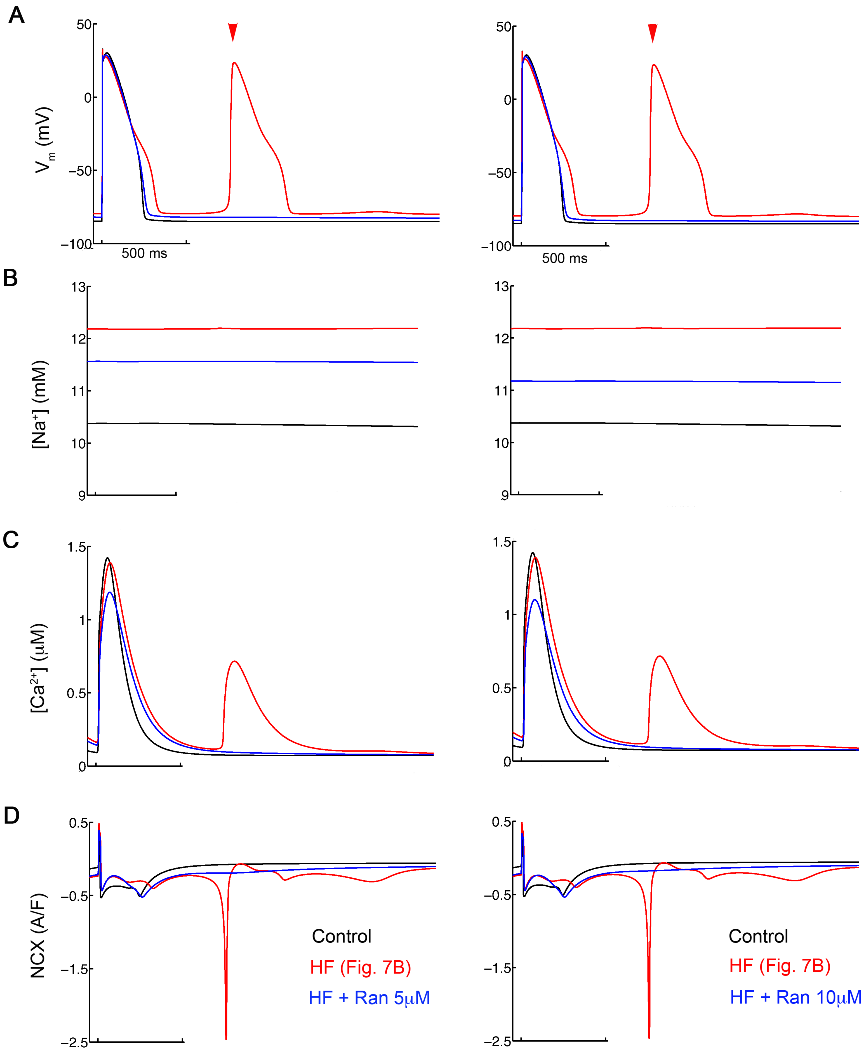

Online Figure VIII: Ionic mechanisms of suppression of triggered activity with application of ranolazine in a HF condition

The HF model (condition from Figure 7B shown here: 10% decreased NKA, 8-fold increased $I_{Na,Leak}$) shown in the red traces displays many characteristic features of heart failure phenotypes found in the literature including (A) increased APD, presence of triggered beats (in this case, DAD – red arrowhead) and diastolic depolarization of the resting membrane potential, (B) an increased Na^+ load, (C) a slight decreased Ca^{2+} transient and blunted decay, and (D) large forward mode NCX generated as a result of increased Ca^{2+} loading. This Ca^{2+} extrusion process depolarizes the membrane potential and leads to I_{Na} activation and a triggered beat. Application of low (5 μM, blue, left column) and high (10 μM, blue, right column) dose ranolazine partly normalizes $[Na^+]_i$ (row B) and forward mode NCX (row D), abolishes the spontaneous Ca^{2+} transient (row C), triggered AP (row A), and partially restores the resting membrane potential, thus elevating the threshold for triggered diastolic events. Many of these results were recently confirmed in a hypertrophic cardiomyopathy experimental model [38]; application of ranolazine shortened the AP, reduced the occurrence of triggered activity, reduced the Ca^{2+} transient and accelerated its decay, and hyperpolarized the resting membrane potential.

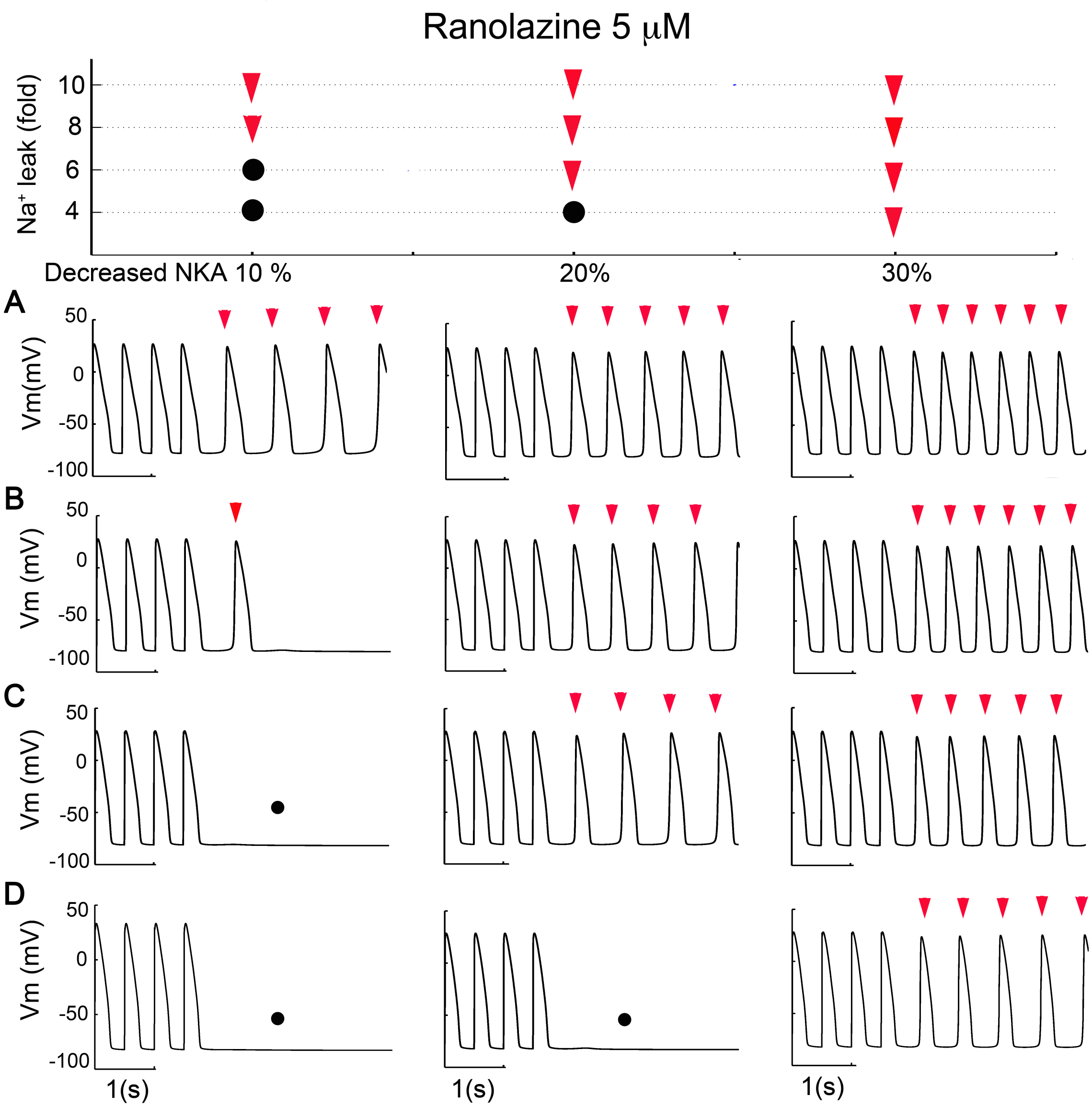

Online Figure IX: DAD abolishment with ranolazine 5 μM when Na^+ leak current is sensitive at an affinity equivalent to *peak* Na^+ current blockade.
Because no data exists for the affinity of ranolazine to the Na^+ leak current, we show both summary data assuming that ranolazine affinity is equivalent to late current affinity (IC_{50} = 6 μM – Figure 7, Online Figures VI – VIII), and here, where ranolazine affinity is assumed equivalent to peak current affinity (IC_{50} = 165.2 μM). As expected, with Na^+ leak current affinity equivalent to peak current affinity (165.2 μM), fewer DADs are abolished, given the same concentration of ranolazine. Row (A) indicates 10-fold Na^+ leak, (B) indicates 8-fold Na^+ leak, (C) indicates 6-fold Na^+ leak, and (D) indicates 4-fold Na^+ leak. Column 1 corresponds to 10% decreased NKA, column 2 is 20% decrease, and column 3 is 30% decrease. Filled black circles (•) indicate absence of DADs, upside down red triangles indicate presence of DADs. See **Supplementary Information** for details on calculation of Na^+ leak current blockade.

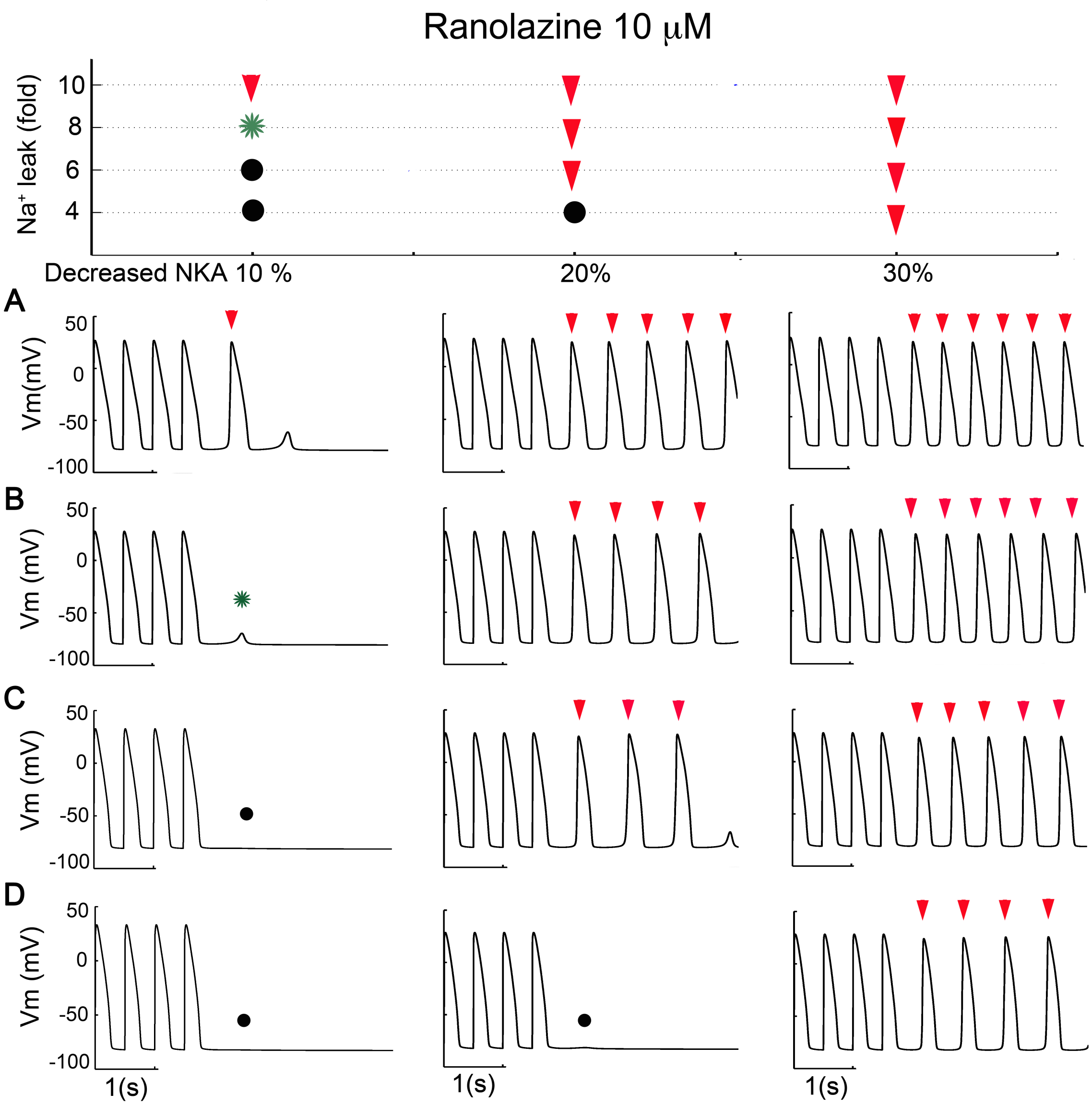

Online Figure X: DAD abolishment with ranolazine 10 μM when Na^+ leak current is sensitive at an affinity equivalent to peak Na^+ current blockade.

Here, we show the same analysis as in Online Figure VII where ranolazine affinity is assumed equivalent to peak current affinity (IC_{50} = 165.2 μM), but with high dose (10 μM) ranolazine. Row (A) indicates 10-fold Na^+ leak, (B) indicates 8-fold Na^+ leak, (C) indicates 6-fold Na^+ leak, and (D) indicates 4-fold Na^+ leak. Column 1 corresponds to 10% decreased NKA, column 2 is 20% decrease, and column 3 is 30% decrease. Filled black circles (•) indicate absence of DADs, upside down red triangles indicate presence of DADs, and green asterisk indicates subthreshold DAD. See **Supplementary Information** for details on calculation of Na^+ leak current blockade.

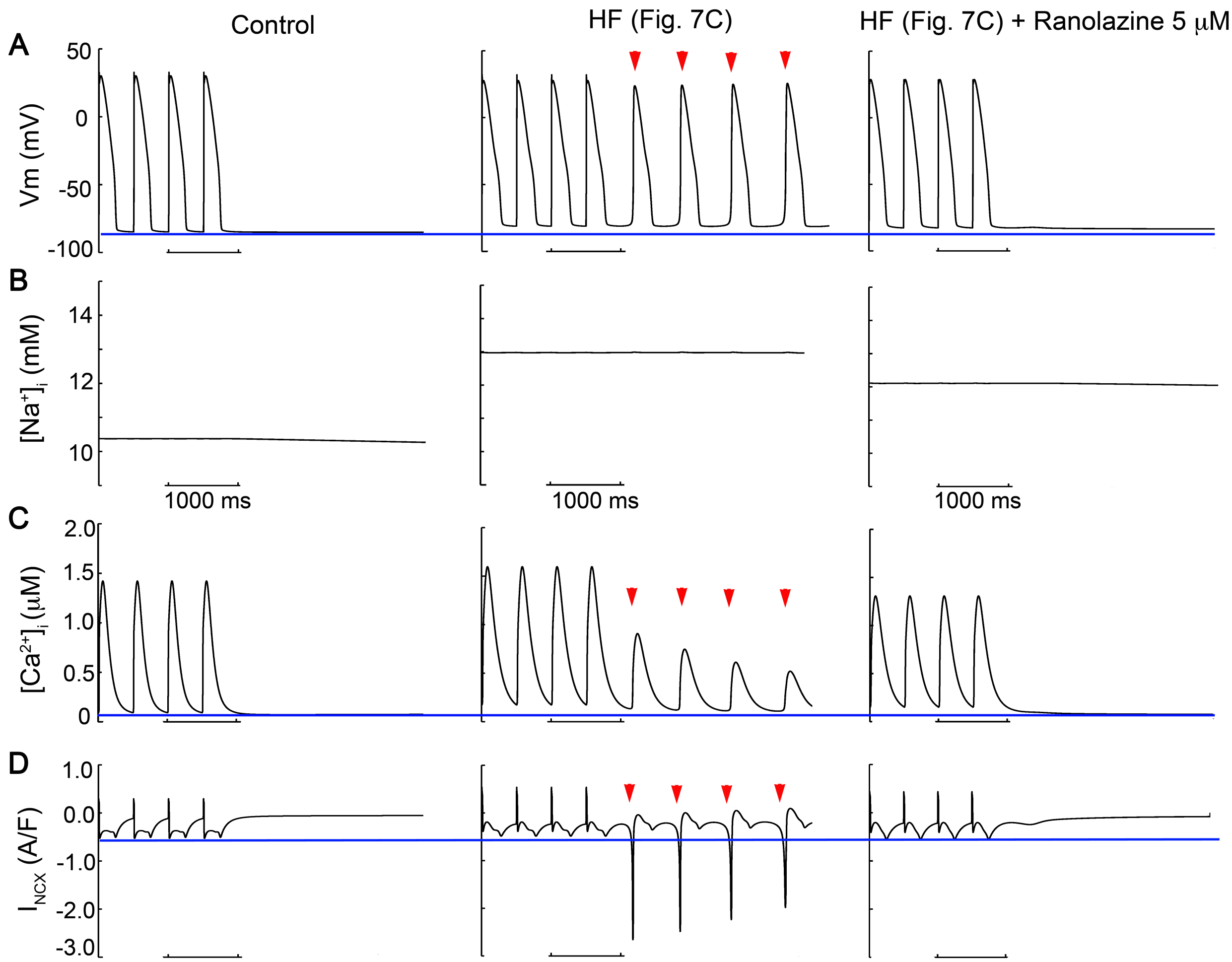

Online Figure XI: Intracellular ion concentrations and expanded analysis for case in Figure 7C (20% decrease NKA, 6-fold increase in Na^+ leak).

Shown in row (A) are cellular APs, (B) intracellular Na^+ concentration, (C) intracellular Ca^{2+} concentration, and (D) Na^+/Ca^{2+} exchange current. Column 1 WT drug-free, column 2 depicts 20% decrease NKA, 6-fold increased Na^+ leak (case C from Figure 7), and columns 3 is the same condition with 5 μM ranolazine. The arrowheads indicate non-paced (DAD) beats. As in Figure 7C, only low dose (5 μM) ranolazine is required to abolish the non-paced DAD beat shown in column 2.

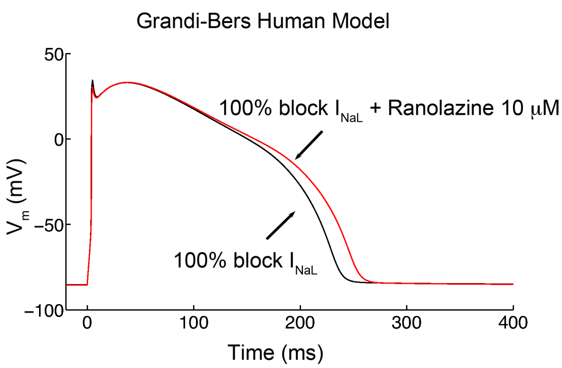

Online Figure XII: Ranolazine application in the absence of late Na^+ current
Action potential (AP) with 100% block of late sodium current (black) and the same condition with ranolazine 10 μM (red) at 1Hz pacing frequencies.

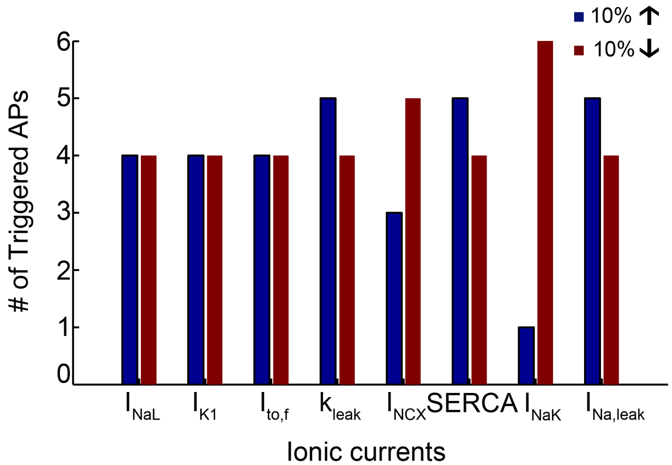

Online Figure XIII: Sensitivity analysis of ionic currents contributing to triggered APs
The current densities changed in the HF were varied by increased or decreased 10%. The baseline model was HF condition of 6-fold increased in Na^+ leak & 20% decreased in NKA, which induced four trigger action potentials. The y-axis indicates number of triggered action potentials.

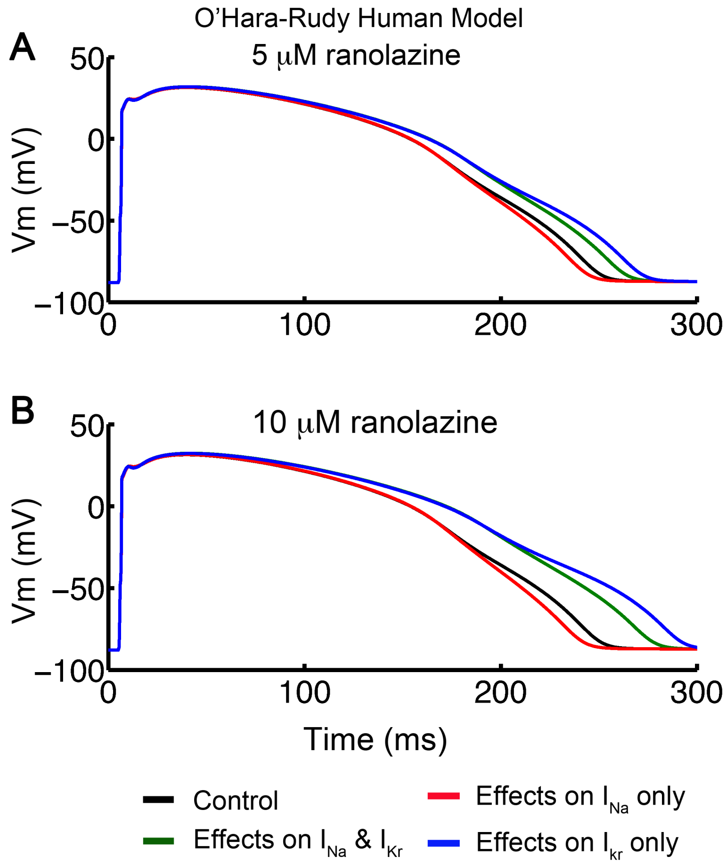

Online Figure XIV: Analysis of composite effects of ranolazine

Here, we show the composite characteristics of ranolazine with I_{Na} and I_{Kr} effects (green) as seen experimentally. We then deconstructed the contributions to each current and show the effects of a hypothetical "pure I_{Na} block ranolazine" (red), or "pure I_{Kr} block ranolazine" (blue). Panels (A) and (B) show the effects of 5 μM and 10 μM, respectively. Consistent with experiments and our hypothesis, a pure I_{Na} block would serve to *decrease* the APD as compared to control (black), and a pure I_{Kr} block would tend to *increase* the APD as compared to control. True ranolazine (simulated in green) shows composite characteristics and lengthens the APD modestly.

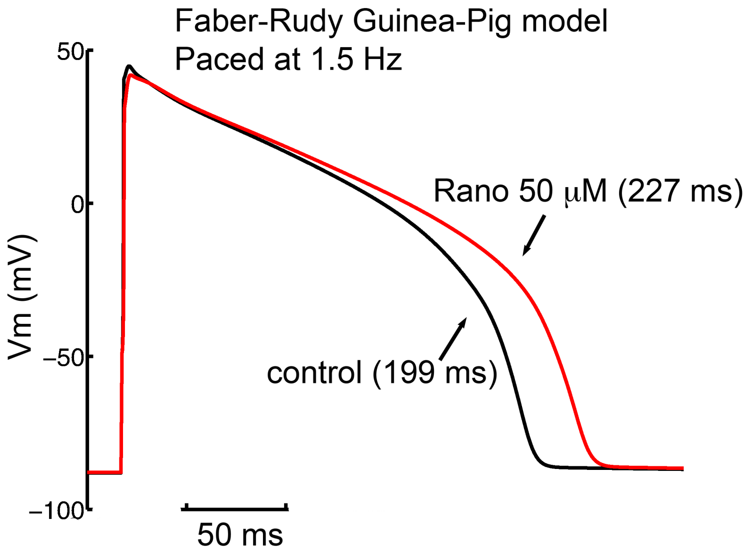

Online Figure XV: Analysis of ranolazine on a simulated guinea-pig ventricular myocyte
To compare APD prolongation with experimental data [39], we simulated the effects of 50 μM ranolazne on a simulated guinea-pig ventricular myocyte model [40] at 1.5 Hz. Consistent with experiments, ranolazine lengthens the APD by 14% (as compared to 22% experimentally).

REFERENCES

1. Moreno JD, Zhu ZI, Yang PC, Bankston JR, Jeng MT, Kang C, Wang L, Bayer JD, Christini DJ, Trayanova NA, Ripplinger CM, Kass RS, Clancy CE. A computational model to predict the effects of class I anti-arrhythmic drugs on ventricular rhythms. *Sci Transl Med.* 2011;3(98):98ra83.
2. Clancy CE, Tateyama M, Kass RS. Insights into the molecular mechanisms of bradycardia-triggered arrhythmias in long QT-3 syndrome. *J Clin Invest.* 2002;110(9):1251-1262.
3. Liu H, Tateyama M, Clancy C, Abriel H, Kass R. Channel Openings Are Necessary but not Sufficient for Use-dependent Block of Cardiac Na+ Channels by Flecainide Evidence from the Analysis of Disease-linked Mutations. *Journal of General Physiology.* 2002;120(1):39-51.
4. Chandra R, Starmer CF, Grant AO. Multiple effects of KPQ deletion mutation on gating of human cardiac Na+ channels expressed in mammalian cells. *Am J Physiol.* 1998;274(5 Pt 2):H1643-1654.
5. Rivolta I, Abriel H, Tateyama M, Liu H, Memmi M, Vardas P, Napolitano C, Priori SG, Kass RS. Inherited Brugada and long QT-3 syndrome mutations of a single residue of the cardiac sodium channel confer distinct channel and clinical phenotypes. *J Biol Chem.* 2001;276(33):30623-30630.
6. An RH, Bangalore R, Rosero SZ, Kass RS. Lidocaine block of LQT-3 mutant human Na+ channels. *Circ Res.* Vol 79; 1996:103-108.
7. Clancy CE, Zhu ZI, Rudy Y. Pharmacogenetics and anti-arrhythmic drug therapy: a theoretical investigation. *American Journal of Physiology- Heart and Circulatory …*; 2007.
8. O'Hara T, Virag L, Varro A, Rudy Y. Simulation of the undiseased human cardiac ventricular action potential: model formulation and experimental validation. *PLoS Comput Biol.* 2011;7(5):e1002061.
9. ten Tusscher KH, Panfilov AV. Alternans and spiral breakup in a human ventricular tissue model. *Am J Physiol Heart Circ Physiol.* 2006;291(3):H1088-1100.
10. Grandi E, Pasqualini FS, Bers DM. A novel computational model of the human ventricular action potential and Ca transient. *J Mol Cell Cardiol.* 2010;48(1):112-121.
11. Bennett PB, Yazawa K, Makita N, George AL. Molecular mechanism for an inherited cardiac arrhythmia. *Nature.* Vol 376; 1995:683-685.
12. Antzelevitch C, Belardinelli L, Zygmunt AC, Burashnikov A, Di Diego JM, Fish JM, Cordeiro JM, Thomas G. Electrophysiological effects of ranolazine, a novel antianginal agent with antiarrhythmic properties. *Circulation.* 2004;110(8):904-910.
13. Rajamani S, Shryock JC, Belardinelli L. Rapid kinetic interactions of ranolazine with HERG K+ current. *J Cardiovasc Pharmacol.* 2008;51(6):581-589.
14. Bennett PB, Valenzuela C, Chen LQ, Kallen RG. On the molecular nature of the lidocaine receptor of cardiac Na+ channels. Modification of block by alterations in the alpha-subunit III-IV interdomain. *Circ Res.* 1995;77(3):584-592.
15. Zhu Y. Flecainide sensitivity of a Na channel long QT mutation shows an open-channel blocking mechanism for use-dependent block. *AJP: Heart and Circulatory Physiology.* Vol 291; 2006:H29-H37.
16. Colquhoun D, Dowsland KA, Beato M, Plested AJ. How to impose microscopic reversibility in complex reaction mechanisms. *Biophys J.* 2004;86(6):3510-3518.

17. Yue DT, Lawrence JH, Marban E. Two molecular transitions influence cardiac sodium channel gating. *Science.* 1989;244(4902):349-352.
18. Liu H. Common Molecular Determinants of Flecainide and Lidocaine Block of Heart Na+ Channels: Evidence from Experiments with Neutral and Quaternary Flecainide Analogues. *The Journal of General Physiology.* 2003;121(3):199-214.
19. Soltis AR, Saucerman JJ. Synergy between CaMKII substrates and beta-adrenergic signaling in regulation of cardiac myocyte Ca(2+) handling. *Biophys J.* 2010;99(7):2038-2047.
20. Fulop L, Banyasz T, Magyar J, Szentandrassy N, Varro A, Nanasi PP. Reopening of L-type calcium channels in human ventricular myocytes during applied epicardial action potentials. *Acta physiologica Scandinavica.* 2004;180(1):39-47.
21. Glukhov AV, Fedorov VV, Lou Q, Ravikumar VK, Kalish PW, Schuessler RB, Moazami N, Efimov IR. Transmural dispersion of repolarization in failing and nonfailing human ventricle. *Circ Res.* 2010;106(5):981-991.
22. Lou Q, Fedorov VV, Glukhov AV, Moazami N, Fast VG, Efimov IR. Transmural Heterogeneity and Remodeling of Ventricular Excitation-Contraction Coupling in Human Heart Failure. *Circulation.* 2011.
23. Plonsey RB, RC. *Bioelectricity: A Quantitative Approach*. New York: Plenum; 1988.
24. Gima K, Rudy Y. Ionic current basis of electrocardiographic waveforms: a model study. *Circ Res.* 2002;90(8):889-896.
25. Zhu ZI, Clancy CE. L-type Ca2+ channel mutations and T-wave alternans: a model study. *Am J Physiol Heart Circ Physiol.* 2007;293(6):H3480-3489.
26. Despa S, Bossuyt J, Han F, Ginsburg KS, Jia LG, Kutchai H, Tucker AL, Bers DM. Phospholemman-phosphorylation mediates the beta-adrenergic effects on Na/K pump function in cardiac myocytes. *Circ Res.* 2005;97(3):252-259.
27. Hoch B, Meyer R, Hetzer R, Krause EG, Karczewski P. Identification and expression of delta-isoforms of the multifunctional Ca2+/calmodulin-dependent protein kinase in failing and nonfailing human myocardium. *Circ Res.* 1999;84(6):713-721.
28. Maltsev VA, Undrovinas AI. A multi-modal composition of the late Na+ current in human ventricular cardiomyocytes. *Cardiovasc Res.* 2006;69(1):116-127.
29. Nabauer M, Beuckelmann DJ, Uberfuhr P, Steinbeck G. Regional differences in current density and rate-dependent properties of the transient outward current in subepicardial and subendocardial myocytes of human left ventricle. *Circulation.* 1996;93(1):168-177.
30. Beuckelmann DJ, Nabauer M, Erdmann E. Alterations of K+ currents in isolated human ventricular myocytes from patients with terminal heart failure. *Circ Res.* 1993;73(2):379-385.
31. Koumi S, Backer CL, Arentzen CE. Characterization of inwardly rectifying K+ channel in human cardiac myocytes. Alterations in channel behavior in myocytes isolated from patients with idiopathic dilated cardiomyopathy. *Circulation.* 1995;92(2):164-174.
32. Hasenfuss G, Reinecke H, Studer R, Meyer M, Pieske B, Holtz J, Holubarsch C, Posival H, Just H, Drexler H. Relation between myocardial function and expression of sarcoplasmic reticulum Ca(2+)-ATPase in failing and nonfailing human myocardium. *Circ Res.* 1994;75(3):434-442.

33. Shannon TR, Wang F, Bers DM. Regulation of cardiac sarcoplasmic reticulum Ca release by luminal [Ca] and altered gating assessed with a mathematical model. *Biophys J.* 2005;89(6):4096-4110.

34. Wagner S, Ruff HM, Weber SL, Bellmann S, Sowa T, Schulte T, Anderson ME, Grandi E, Bers DM, Backs J, Belardinelli L, Maier LS. Reactive oxygen species-activated Ca/calmodulin kinase IIdelta is required for late I(Na) augmentation leading to cellular Na and Ca overload. *Circ Res.* 2011;108(5):555-565.

35. Bundgaard H, Kjeldsen K. Human myocardial Na,K-ATPase concentration in heart failure. *Mol Cell Biochem.* 1996;163-164:277-283.

36. Bossuyt J, Ai X, Moorman JR, Pogwizd SM, Bers DM. Expression and phosphorylation of the na-pump regulatory subunit phospholemman in heart failure. *Circ Res.* 2005;97(6):558-565.

37. Shamraj OI, Grupp IL, Grupp G, Melvin D, Gradoux N, Kremers W, Lingrel JB, De Pover A. Characterisation of Na/K-ATPase, its isoforms, and the inotropic response to ouabain in isolated failing human hearts. *Cardiovasc Res.* 1993;27(12):2229-2237.

38. Coppini R, Ferrantini C, Yao L, Fan P, Del Lungo M, Stillitano F, Sartiani L, Tosi B, Suffredini S, Tesi C, Yacoub M, Olivotto I, Belardinelli L, Poggesi C, Cerbai E, Mugelli A. Late sodium current inhibition reverses electromechanical dysfunction in human hypertrophic cardiomyopathy. *Circulation.*127(5):575-584.

39. Wu L, Shryock JC, Song Y, Li Y, Antzelevitch C, Belardinelli L. Antiarrhythmic effects of ranolazine in a guinea pig in vitro model of long-QT syndrome. *J Pharmacol Exp Ther.* 2004;310(2):599-605.

40. Faber GM, Rudy Y. Action potential and contractility changes in [Na(+)](i) overloaded cardiac myocytes: a simulation study. *Biophys J.* 2000;78(5):2392-2404.